urther quasicomponent distribution function analysis of quid water. Temperature dependence of the results

Mihaly Mezei and David L. Beveridge

Chemistry Department, Hunter College of the City University of New York, New York, New York 10021
(Received 29 December 1980; accepted 10 February 1981)

Metropolis Monte Carlo computer simulation results are presented for liquid water as represented by the MCY and ST2 potentials to study the temperature dependence of the calculated internal energy, heat capacity, pressure, and the molecular distribution functions and to present the hydrogen–oxygen and hydrogen–hydrogen radial distribution functions, the distribution of the near-neighbor dipole angles and pair energies, the size distribution of cavities in the liquid, and the radial distribution function for molecules with a given coordination number. A detailed comparison with available experimental data documents the degree of agreement to be expected from computations at this level of approximation and characterizes the sensitivity of results to the choice of intermolecular potential function. The simulations performed at 37 and 50 °C on the MCY water at the corresponding experimental densities reveal a small but significant shift in the direction of structure loss when compared with our previous results at 25 °C.

I. INTRODUCTION

In a series of recent paper from this Laboratory,[1–4] we have described the structure of liquid water as determined from Metropolis Monte Carlo computer simulation assuming pairwise additive intermolecular interactions. The focus in this work has been on the compositional analysis of the system in terms of quasicomponent distribution functions (QCDF)[5] for coordination number, binding energy and hydrogen-bonding characteristics, and on the characterization of the convergence properties of the Metropolis method as applied to molecular liquids.

The purpose of the present paper is twofold. First, the temperature dependence of the MCY water properties is investigated by comparing the results obtained for 25 °C with the results of two new Monte Carlo calculations performed at 37 and 50 °C. Second, the previously presented description of liquid water based on the MCY (Ref. 6) and ST2 (Ref. 7) intermolecular potentials is extended to include consideration of hydrogen–oxygen and hydrogen–hydrogen radial distribution functions, the distribution of the near-neighbor dipole angles and pair energies, the size distribution of cavities in the liquid, and the radial distribution function for molecules with a given coordination number. Also, quantitative calculations of the pressure for MCY and ST2 waters are reported.

Section II presents the background and the motivations for the present work, Sec. III describes the theory involved, and Sec. IV gives the details of the Monte Carlo calculations and their analyses. The results are presented and discussed in Sec. V. Section VI gives a summary and the conclusions drawn from the results.

II. BACKGROUND

Liquid water has been the focus of a considerable number of computer simulation studies in recent years both from the probabilistic Monte Carlo point of view and from the deterministic method of molecular dynamics. This work is summarized in several current reviews from this group[8,9] and other laboratories.[10,11] In this section we briefly review the results obtained in our previous papers and closely related works relevant to the consideration of the present study in context.

This series of studies began with a (T, V, N) ensemble liquid water computer simulation based on the MCY potential function carried out for a temperature of 25 °C, at a volume commensurate with the observed density. Ensemble averages initially reported[1] were based on 500 K configurations for 125 molecules under periodic boundary conditions, subsequently extended to 4400 K configurations to validate convergence and also for further study of the convergence problem.[3] The calculated thermodynamic internal energy from the 4400 K realizations was -8.65 ± 0.3 kcal/mol, compared with an observed value of -9.9 kcal/mol. The discrepancy of ~13% was ascribed mainly to the assumption of pairwise additivity in the configurational potential. The calculated heat capacity was found to be 20.1 cal/mol deg versus a measured value of 18 cal/mol deg at 25 °C. The calculated pressure was reported to be considerably in error,[12] indicative of the limitations yet remaining in the shape of the configurational potential.

Our analysis of the structure of liquid water was carried out in terms of the radial distribution function $g(R)$ and the QCDF's $x_C(K)$ for coordination number K and $x_B(\nu)$ for binding energy ν. This general approach to structure defined on the statistical state of the system had recently been systematically formalized by Ben-Naim,[5] and the water structure problem had been associated with the modality of $x_B(\nu)$ (Ref. 13). The calculated $x_B(\nu)$ for liquid water in our simulations was found to be continuous and unimodal, and thus supportive of the energetic continuum model for the structure of liquid water. A similar result was simultaneously obtained from (T, P, N) Monte Carlo computer simulation by Owicki and Scheraga.[14] The Rahman–Stillinger molecular dynamics calculation produced a continuous distribution of hydrogen-bond energies with similar implications about the continuum model. Examination of computer-drawn stereographic views of significant mo-

 0021-9606/82/010593-08$02.10

lecular structures extracted from the liquid water simulation confirms a notable prevalence of bent hydrogen bonds in the system.

In subsequent work in the area of liquid water structure, we reported[4] a detailed analysis of the structure of liquid water in terms of QCDF's based explicitly on hydrogen-bond indices. The average intermolecular hydrogen-bond angle was found to be ~20°, in close accord with Pople's 1951 assumption in the original continuum model paper[15] and the value recently inferred from vibrational spectroscopic data by Sceats *et al.*[16] This result is supported by Jorgensen's analysis of the hydrogen-bond structure[17] of his water model.[18] The extent of hydrogen-bond networks in our simulated water as determined by the network analysis approach devised by Geiger, Rahman, and Stillinger[19] revealed, in agreement with their results based on molecular dynamics computer simulation using the ST2 potential, that for any reasonable definition of a water–water hydrogen bond, all molecules of the system are tied up in the net; i.e., the number of water monomers in the system is negligibly small. The most recent and definitive spectroscopic results on liquid water fully support this conclusion.[20] In summary, the structural view of liquid water emergent from this work and of all related computer simulation studies from other laboratories is that the statistical state of the system is best described as a fully developed network of water molecules interacting via bent hydrogen bonds.

The above description of the structure of liquid water is supplemented in the present paper by the calculation of a number of other quantities obtainable from the analysis of our Monte Carlo simulations. The distribution of the relative orientations of neighboring water molecules gives important indications as to the nature of the water–water intermolecular interactions and quantifies the localizing effect of both the hydrogen-bond and the dipolar interaction. In the previous work, the relative orientations were characterized in terms of the hydrogen-bond angle QCDF's, $x_H(\theta_H)$ and $x_H(\theta_{LP})$ (Ref. 4). The present work gives a complementary characterization in terms of the dipole angle correlations, using the QCDF $x_D(\theta_D)$.

In the study of the composition in terms of energetic indices, the unimodal nature of the QCDF of the binding energy was found to be of great importance for deciding the applicability of the early mixture models to liquid water as modeled by the MCY or ST2 potentials.[6,7] Further information on the energetics is available from the QCDF of the pair energy ϵ, $x_P(\epsilon)$, reported for both potential functions herein. Comparison of these results further quantifies the sensitivity of energetic properties of the system to the choice of the potential function.

Joint QCDF's are in general capable to describe more complex structural properties than single (one-parameter) QCDF's. The possible existence of interstitial water, postulated by earlier mixture models can go undetected by the consideration of the $g(R)$ or the $x_C(K)$ only. To examine this problem in more detail, we computed the radial distribution functions for waters with coordination numbers 3, 4, 5, and 6 separately. Any evidence of interstitial waters should appear in the $g(R)$ for the six-coordinated species since a water molecule sitting in the center of an Ice Ih cage would have six neighbors at a distance of 3.0 Å and another six neighbors at a distance of 3.5 Å.

The free energy required to form a cavity of a given size is an important quantity in the theory of solvation, and is closely related to the probability of finding a cavity of that size in the liquid. This latter quantity is readily accessible from the results of a computer simulation and calculation of the cavity distributions in the MCY and ST2 waters are reported herein.

The calculated results on the pressure have frequently been cited to point out deficiencies remaining in the intermolecular potentials. The pressure of the MCY water has been previously reported to be "above 3000 atm."[12] It is of interest to know its actual value, particularly when temperature effects are studied in order to ensure that the changes observed were not greatly influenced by the concomittant pressure change. The results are compared with the ST2 result reported by Rao *et al.*,[21(b)] corrected here with the contribution due to the finite cutoff (see Sec. III). The significance of these results with respect to the calculated structure of the liquid is further discussed.

III. THEORY AND METHODOLOGY

Here we briefly review the standard way of the computation of configurational internal energy, constant volume excess heat capacity, and the pressure from Monte Carlo calculations. The configurational internal energy is obtained as a simple average over the Markov chain,

$$U = \langle E(\mathbf{X}^N)\rangle = (1/M)\sum_{j=1}^{M} E(\mathbf{X}_j^N), \tag{1}$$

where M is the number of configurations in the Markov chain. The notation $\langle\ \rangle$ will be used to denote configurational averaging. The excess constant-volume heat capacity is obtained from the fluctuations in the internal energy over the Markov chain:

$$C_v' = [\langle E(\mathbf{X}^N)^2\rangle - \langle E(\mathbf{X}^N)\rangle^2]/kT^2. \tag{2}$$

Unfortunately, the computation of C_v' is much less reliable from Monte Carlo calculations than that of the internal energy because of the $\langle E(\mathbf{X}^N)^2\rangle$ term[21,3]; in case of liquid water errors of ~40% can be encountered for runs of medium (~1000 K) length.[3]

The pressure can be obtained through the computation of the virial sum:

$$p_0 = (kT/V)\left\{N - \left\langle \sum_{i=1}^{N} [\mathbf{R}_i \cdot \partial E(\mathbf{X}^N)/\partial \mathbf{R}_i]\right\rangle\right\}, \tag{3}$$

where k is the Boltzmann constant, T is the absolute temperature, and $\mathbf{R}_i$ describes the location of molecule i. Furthermore, the discontinuous cutoff applied to the potential gives rise to a correction term that is due to the Dirac δ appearing in the derivative of the pair energy $E^{(2)}(R)$ at $R = R_{max}$:

$$p_C = (2\pi/3)\rho^2 R_{max}^3 \langle E^{(2)}(R_{max})\rangle_\Omega\, g(R_{max}), \tag{4}$$

here $\langle\ \rangle_\Omega$ denotes configurational averaging over the relative orientations of two molecules. In general, $\langle E^{(2)}(R_{max})\rangle_\Omega g(R_{max})$ can be estimated from the Monte Carlo calculation as

$$\langle E^{(2)}(R)\rangle_\Omega g(R) = \langle E^{(2)}(R, R+\Delta R)\rangle_\Omega / 4\pi R^2 \Delta R, \quad (5)$$

where $\langle E^{(2)}(R, R+\Delta R)\rangle$ is the average of the pair energies for any given molecule with all other molecules whose distance from this molecule is between R and $R+\Delta R$. In the case of the MCY potential two such correction terms arise, one from the cutoff applied to the exponential terms (at $R_{max}=5.82$ Å) and an other from the cutoff applied to the $1/r$ terms (at $R_{max}=7.75$ Å), denoted by p'_C and p''_C, respectively.

The distribution functions not defined previously in the QCDF formalism are; near-neighbor dipole angle correlation $x_D(\theta_D)$, near-neighbor pair energy $x_p(\epsilon)$, cavities $x_0(R_C)$ and radial distribution function for molecules with fixed coordination number $g(K, R)$. The near-neighbor dipole correlation function $x_D(\theta_D)$ is computed for water pairs with center-of-mass distance less than or equal to R_M, the radius of the first solvation shell. This function is defined as

$$x_D(\theta_D) = \int_V \sum_{i<j}^{N} \delta[\theta_D^{ij}(\mathbf{X}^N) - \theta_D] P(\mathbf{X}^N) C^{ij}(\mathbf{X}^N) d\mathbf{X}^N / \int_V \sum_{i<j}^{N} P(\mathbf{X}^N) C^{ij}(\mathbf{X}^N) d\mathbf{X}^N, \quad (6)$$

where θ_D is the angle between the HOH bisectors, $\theta_D^{ij}(\mathbf{X}^N)$ is the angle between the dipoles of the molecules i and j, $\delta[\ ]$ is the dirac delta, $C^{ij}(\mathbf{X}^N)$ is one if the distance between i and j is less than R_M and zero otherwise, and $P(\mathbf{X}^N)$ is the probability of the occurrence of the configuration $\mathbf{X}^N$. The normalized distribution, $x_D(\theta_D)/\sin\theta_D$ is also of interest since the normalization factors out the effect of the difference in the volume of configuration space corresponding to different θ_D values.

Next we consider the distribution of the pair energies. This quantity is usually presented for all pairs of particles in the system. It has the disadvantage, however, that the large peak around zero, corresponding to the distant pairs, tends to dominate the curve. The quantity of principal interest, the peak corresponding to the optimum near-neighbor distance may only appear as a shoulder in this distribution. However, by including only near-neighbor water pairs (that is, waters whose distance is R_M or less), the dominant feature of the curve will be the peak corresponding to the optimum near-neighbor distance,[6] and the interpretation is then straightforward. The distribution function $x_p(\epsilon)$ is then defined as

$$x_p(\epsilon) = \int_V \sum_{i<j}^{N} \delta[\epsilon^{ij}(\mathbf{X}^N) - \epsilon] P(\mathbf{X}^N) C^{ij}(\mathbf{X}^N) d\mathbf{X}^N / \int_V \sum_{i<j}^{N} P(\mathbf{X}^N) C^{ij}(\mathbf{X}^N) d\mathbf{X}^N, \quad (7)$$

where $\epsilon^{ij}(\mathbf{X}^N)$ is the value of the pair energy between the molecules i and j.

The distribution of cavities can be obtained by generating uniformly distributed test points and finding the distance of the closest water molecule to each test point. To avoid arbitrary definition of the molecular radius the distribution of the distance to the nearest water center-of-mass is given. Thus the actual cavity size is obtained by deducting the assumed molecular radius of water from the distances shown here. The distribution function $x_0(R_C)$ is defined as

$$x_0(R_C) = \int_V \lim_{\Delta R \to 0} C(\mathbf{X}, R_C, \Delta R_C)/\Delta R_C\, d\mathbf{X}/V. \quad (8)$$

$$C(\mathbf{X}, R, \Delta R) = \begin{cases} \text{if } R < \min_i |\mathbf{X}_i - \mathbf{X}| \le R + \Delta R \text{ then: } 1 \\ \text{otherwise: } 0, \end{cases} \quad (9)$$

where the $\mathbf{X}_i$ are the coordinates of the centers of masses of the molecules.

The radial distribution function for different coordination numbers, $g(K, R)$ is defined as

$$g(K, R) = \lim_{\Delta R \to 0} N(K, R, R+\Delta R)/[4\pi R^2 \Delta R \rho x_C(K)], \quad (10)$$

where $N(K, R, R+\Delta R)$ is the number of water molecules whose distance from a water with coordination number K falls between R and $R+\Delta R$, ρ is the bulk density, and $x_C(K)$ is the mole fraction of molecules with coordination number K.

IV. CALCULATIONS

The results presented in this paper are based on the previously reported Monte Carlo calculations on the MCY and ST2 waters at 25 and 10 °C, respectively,[3] and on two new calculations on the MCY water at 37 and 50 °C described here the first time. The system size, length of the run, potential functions used, temperature and the boundary conditions applied are summarized in Table I. All systems were studied at their experimental

TABLE I. Specification of the Monte Carlo calculations analyzed. The length of the run is in the unit of 1000 steps. sc stands for simple cubic and fcc stands for face-centered cubic periodic boundary conditions. Runs 1, 4, and 5 are described in Ref. 3.

	Water–Water potential	N	Length	Boundary conditions	Temp.	ρ (g/ml)
1	MCY	125	4400 K	sc	25 °C	0.997
2	MCY	216	1500 K	fcc	37 °C	0.993 360
3	MCY	216	2200 K	fcc	50 °C	0.988 066
4	ST2	216	4900 K	sc	10 °C	1.000
5	ST2	155	1900 K	fcc	10 °C	1.000

TABLE II. Bulk thermodynamic properties as a function of temperature and potential. The energy is given in kcal/mol, the heat capacity in cal/mol deg and the pressure in atm. The value for p_0 of the ST2 water is computed from the $pV/\rho kT - 1 = -0.023$ given by [Ref. 21(b)]. The p_C' value for the ST2 water was computed from our ST2 run (Ref. 3). The segments B and C refer to the grand cycle found in the very long MCY run at $T = 25\,°C$.

	U	C_v'	p_0	p_C'	p_C''	p
Segment B	-8.56 ± 0.03					
Segment C	-8.64 ± 0.03					
25°C	-8.65 ± 0.1	11.5 ± 2	7552 ± 238	-70 ± 1	-722 ± 200	6760 ± 311
37°C	-8.57 ± 0.04	14.0 ± 1	7928 ± 233	-69 ± 1	-937 ± 188	6922 ± 299
50°C	-8.40 ± 0.03	13.0 ± 2	8017 ± 148	-70 ± 1	-769 ± 124	7178 ± 193
ST2	-10.6	20.6	1232		-689	543

densities, with the exception of the ST2 water where $\rho = 1.000$ g/ml was used to remain consistent with previous calculations.

The computed distribution functions from the Monte Carlo run were based in every $4N$th configurations, where N is the number of molecules considered. This involves negligible loss of information since the change between two configurations involve at most one molecule and thus the successive configurations are strongly correlated. We have determined by comparing the results with more frequent averaging at selected points that errors from this source in the QCDF's are less than 1%.

The statistical uncertainties in the computed expectation values and QCDF's can be estimated in different ways. The previous very long (4400 K) calculation at $T = 25\,°C$ on the MCY water showed the emergence of certain "grand cycles" of very large (~1500 K) period and small amplitude (~2%). The values of a given quantity over two different parts of the grand cycle can provide a lower and upper bound for the total average. This method was used for some of the 25 °C MCY run. In most of the cases the method described by Wood was applied together with a statistical test to ensure that the block averages used for the error estimate are uncorrelated. For the estimation of the error in C_v' neither of the above methods are suitable. An approximate estimate can be obtained from the amplitude of the oscillations in the curve of C_v' as a function of the length of the calculation.

V. RESULTS AND DISCUSSION

The control functions of the two calculations are displayed on Figs. 1 and 2. The grand cycles found at the 25 °C calculation are also in evidence here and ensemble averages from our calculations cover approximately one full cycle at each temperature. Based on our experiences gained from the previous very long runs we expect that the improvement of accuracy using much longer runs would be marginal for most of the properties discussed.

Our results for the thermodynamic properties of MCY water are collected in Table II. The internal energy increases (get less negative) with the increase of temperature, as expected. The excess constant-volume heat capacity C_v' shows a maximum at $T = 37\,°C$, but the error bounds on these values are larger than the differences and this behavior can not be considered statistically significant.

The calculated pressure requires some special comments. Lie, Clementi, and Yoshimine estimated[12] that the pressure of the MCY water in their Monte Carlo simulations was "above 3000 atm." The 6760 atm obtained in this study confirms this point. The results on the temperature dependence of the pressure provide an added reason for caution in the evaluation of the temper-

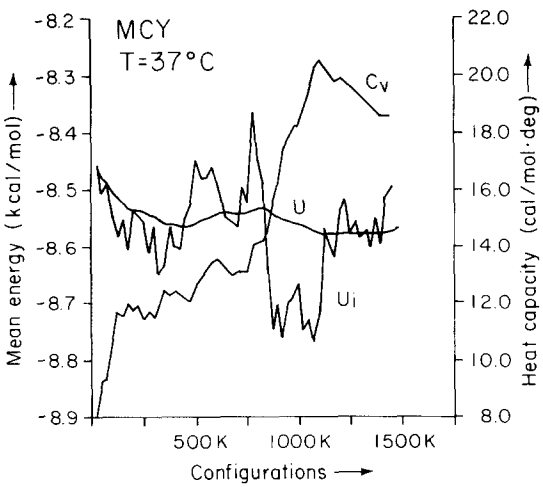

FIG. 1. Convergence of U and C_v' of the MCY water at 37 °C. The control function U_i is computed using 25 K block averages.

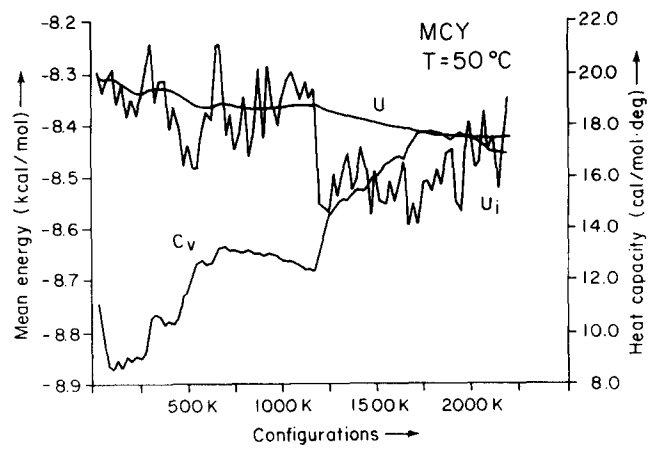

FIG. 2. Convergence of U and C_v' of the MCY water at 50 °C. The control function U_i is computed using 25 K block averages.

ABLE III. Description of the center-of-mass radial distribution function as a function of temperature nd potential. The segments A and B refer to two phases of the grand cycle found in the very long MCY un at $T = 25\,^{\circ}C$. The radial distances are in Å. Experimental distribution function refers to oxygen–xygen distances.

	g (r max1)	r max1	g (r min1)	r min1	g (r max2)	r max2
MCY Segment A	2.59	2.82	0.98	3.45	1.09	4.20
MCY Segment B	2.67	2.80	0.92	3.40	1.12	4.25
MCY 25 °C	2.62	2.85	0.964	3.40	1.09	4.05
MCY 37 °C	2.51	2.80	0.965	3.45	1.08	4.15
MCY 50 °C	2.45	2.80	0.972	3.50	1.08	4.30
ST2 10 °C	3.31	2.80	0.64	3.425	1.22	4.60
EXP 25 °C	2.33	2.85	0.851	3.55	1.132	4.65
EXP 50 °C	2.28	2.85	0.969	3.40	1.115	4.75

TABLE IV. Description of the hydrogen–oxygen radial distribution function as a function of temperature and potential. The segments B and C refer to two phases of the grand cycle found in the very long MCY run at $T = 25\,^{\circ}C$. The radial distances are in Å. MD: Ref. 7, molecular dynamics; MC: Ref. 21(b), Monte Carlo.

	g (r max1)	r max1	g (r min1)	r min1	g(r max2)	r max2
MCY Segment B	1.185	1.90	0.252	2.50	1.718	3.30
MCY segment C	1.136	1.90	0.272	2.50	1.714	3.35
MCY 25 °C	1.156	1.90	0.264	2.50	1.715	3.30
MCY 37 °C	1.112	1.90	0.283	2.50	1.682	3.35
MCY 50 °C	1.070	1.90	0.305	2.50	1.652	3.30
ST2 10 °C MD	1.39	1.83	0.29	2.35	1.61	3.32
ST2 10 °C MC	1.40	1.98	0.34	2.38	1.60	3.22

TABLE V. Description of the hydrogen–hydrogen radial distaibution function as a function of temperature and potential. The segments B and C refer to two phases of the grand cycle found in the very long MCY run at $T = 25\,^{\circ}C$. The radial distances are in Å. MD: Ref. 7, molecular dynamics; MC: Ref. 21(b), Monte Carlo.

	g ($r$max1)	r max1	g (r min1)	r min1	g (r max2)	r max2
MCY Segment B	1.459	2.45	0.851	3.10	1.237	3.80
MCY Segment C	1.430	2.45	0.870	3.10	1.230	3.80
MCY 25 °C	1.443	2.45	0.864	3.10	1.231	3.80
MCY 37 °C	1.417	2.45	0.881	3.10	1.216	3.80
MCY 50 °C	1.400	2.45	0.886	3.10	1.208	3.80
ST2 10 °C MD	1.51	2.46	0.77	2.98	1.16	3.92
ST2 10 °C MC	1.53	2.33	0.77	3.04	1.15	3.83

ature dependence of expectation values in general from Monte Carlo calculations. The rather large correction terms obtained for the pressure further indicate that while Eqs. (3) and (4) are adequate to obtain an approximate value for the pressure, it is difficult to obtain an accurate estimate for potentials with a discontinuous cutoff since the correction term p_C is in general negative and rather large.

The present result on the pressure of the MCY water at the experimental density at 25 °C can be combined with the result of Owicki and Scheraga on the volume of the MCY water at the experimental pressure[14] to provide an estimate for the isothermal compressibility, χ_T, at 25 °C. Assuming that χ_T is independent of the pressure, we obtain

$$\chi_T \approx [(V_1 - V_2)/V_1]/(P_2 - P_1)\,. \tag{11}$$

Using $(V_1 - V_2)/V_1 = 0.24$ (Ref. 14) and $P_2 - P_1 = 6760 - 1$ atm, we obtain $\chi_T = 3.6 \times 10^5$ atm^{-1}. This compares reasonably well with the experimental value, 4.62×10^5 atm^{-1}.

The location and the values of the first three extrema of the center-of-mass radial distribution functions are given in Table III. The changes found are in good agreement with the changes in the experimental results of Narten[22]: The increase in temperature lowers the first maximum, raises the first minimum and shifts the location of the second maximum to a larger distance. The hydrogen–oxygen and hydrogen–hydrogen radial distribution functions are shown on Fig. 3 for the MCY water at 25 °C. The locations and the values of the first three extrema are collected in Tables IV and V, respectively, for all the temperatures studied. Corresponding results

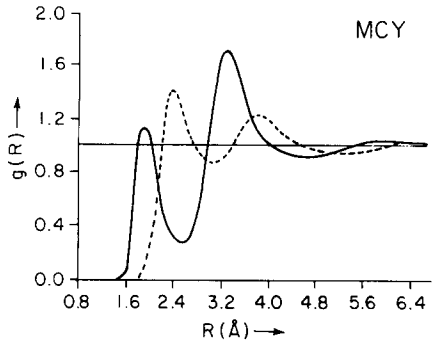

FIG. 3. Hydrogen–oxygen (full line) and hydrogen–hydrogen radial distribution functions (broken line) for the MCY water at 25 °C.

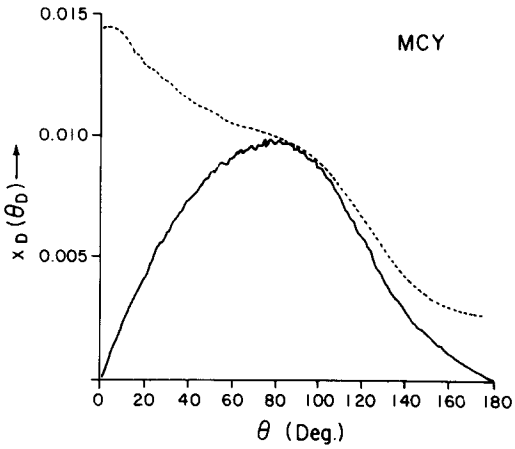

FIG. 4. Near-neighbor dipole-correlation functions for MYC water at $T = 25$ °C. Full line: $x_D(\theta_D)$: dotted line: $x_D(\theta_D)/\sin\theta_D$.

on the ST2 water are also shown based on Refs. 7 and 21(b).

Table VI contains the values of $x_C(3)$, $x_C(4)$, and $x_C(5)$ at various temperatures. In this case there are two opposing effects present. The increase in the temperature in general increases the density fluctuations in a liquid. As a consequence, the average coordination number should decrease, thus giving rise to a higher frequency of low water coordination number. On the other hand, the generally low coordination number is a consequence of the strongly directional hydrogen bonding forces whose effect should decrease with the increase in the temperature. The results show a statistically significant increase in $x_C(3)$, indicating that the dominating effect is the increase of the density fluctuations.

The distribution of $x_D(\theta_D)$ and of $x_D(\theta_D)/\sin\theta_D$ are shown on Figs. 4 and 5 for the MCY water at 25 °C and for the ST2 water at 10 °C, respectively. The distributions $x_D(\theta_D)$ are rather wide in both cases, with a flat peak in the range of 45–90°. On the other hand, the distribution $x_D(\theta)/\sin\theta_D$ is essentially bimodal, having a large peak at $\theta_D = 0°$ and a smaller one at $\theta_D = 90°$. The first peak corresponds to a geometry featuring a favorable dipole–dipole interaction while the second one corresponds to the hydrogen-bonding geometry. The significance of the dipole–dipole interaction is further increased for the ST2 water. It should be stressed that the relative magnitude of the two peaks are not representative of the relative significance of the dipolar and hydrogen bonding forces since a given dipole angle θ_D can be realized with a wide range of hydrogen-bond angles θ_H and vice versa. In fact, the curve of $x_H(\theta_H)/\sin\theta_H$ does not even show a second peak that would correspond to the dipolar bond.[4] It might be concluded from the joint consideration of $x_H(\theta_H)$ and $x_D(\theta_D)$ that the particular geometry of the water molecule gives rise to a favorable combination of these two forces to produce a strongly bound network of water molecules in the liquid state. The results at $T = 37$ °C and at $T = 50$ °C (not shown) are similar to the $T = 25$ °C results but the peak representing the hydrogen-bonded interactions became successively smaller, at $T = 50$ °C degenerating into a shoulder. This implies that at higher temperatures the importance of the dipolar forces should increase at the expense of the hydrogen bond.

The distributions of near-neighbor pair energies $x_P(\epsilon)$, are shown on Fig. 6 for both the MCY water at

TABLE VI. Description of the coordination number distributions as a function of temperature and potential. The segments A and B refer to two phases of the grand cycle found in the very long MCY run at $T = 25$ °C.

	x_C (3)	x_C (4)	x_C (5)
MCY Segment A	0.156	0.449	0.288
MCY Segment B	0.146	0.474	0.287
MCY 25 °C	0.151	0.456	0.224
MCY 37 °C	0.216	0.459	0.224
MCY 50 °C	0.230	0.447	0.217
ST2 10 °C	0.049	0.404	0.337

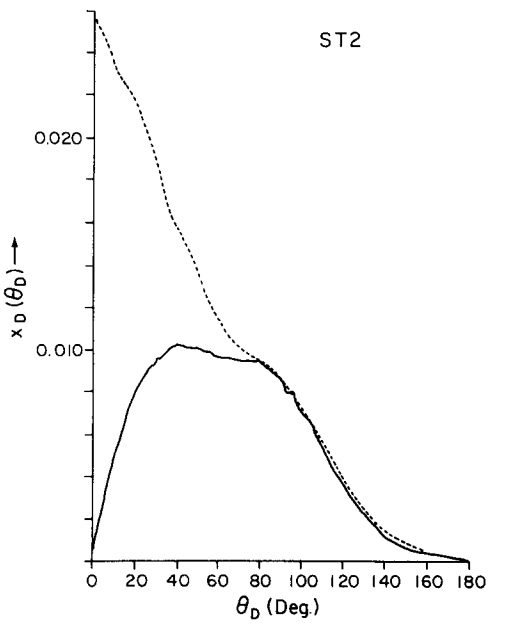

FIG. 5. Near-neighbor dipole-correlation functions for ST2 water at $T = 10$ °C. full line: $x_D(\theta_D)$, dotted line: $x_D(\theta_D)/\sin\theta_D$.

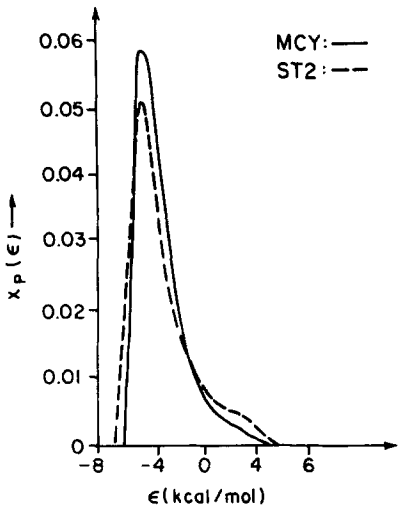

FIG. 6. Distribution of near-neighbor pair energies for both the MCY water at $T=25\,^{\circ}C$ (full line) and the ST2 water at $T=10\,^{\circ}C$ (broken line).

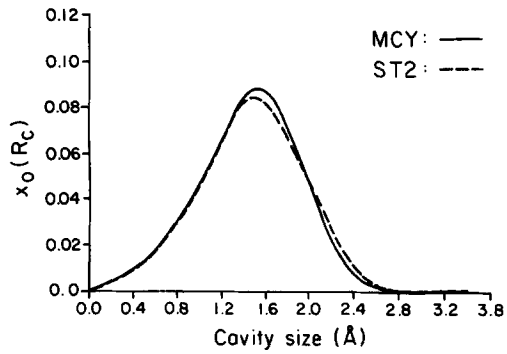

FIG. 7. Probability of finding a cavity of radius R_C for both the MCY water at $T=25\,^{\circ}C$ (full line) and the ST2 water at $T=10\,^{\circ}C$ (broken line).

25 °C and the ST2 water at 10 °C. The dominant feature of both curves is the single sharp peak and a shoulder around 3–4 kcal/mol. This latter is probably due to the cutoff applied for computing the distribution since the contributions to the large positive values came from the very close neighbors while the smaller values can arise from either the very close or the distant neighbors. The increase of temperature has very little effect on $x_p(\epsilon)$: The peak is at −4.4 kcal/mol for $T=25\,^{\circ}C$ and $T=37\,^{\circ}C$, and shifts to −4.3 kcal/mol at $T=50\,^{\circ}C$ as expected (not shown here).

The distribution of cavities of different sizes are shown on Fig. 7 for both the MCY water at 25 °C and the ST2 water at 10 °C. The two curves are rather similar to each other at the first sight, but the difference is larger if the considerations are restricted to $R_C > 2.4$ Å, i.e., to cavities of a size sufficient to accommodate a water molecule. By integrating the distribution from 2.4 Å to infinity, it was found that the probability of finding a cavity larger than 2.4 Å is 0.014 for the MCY water and 0.029 for the ST2 water. This difference is consistent with the larger pressure obtained for the MCY water. The integrated probabilities of finding cavities larger than 2.4, 2.6, and 2.8 Å, respectively, for the different water models are presented in Table VII. The temperature dependence of the cavity distribution is an interesting question since the often postulated icelike clusters would produce a decline in the appearance of molecular sized cavities while arguments valid for regular liquids would imply increased occurrences of the larger cavities due to the increase in the fluctuations in the system. A comparison of the results at different temperatures show a consistent but weak trend toward increased probability of finding molecular sized cavities as the temperature is increased although the changes are not exceeding the error bounds established. This change is consistent with the results on the coordination numbers.

The radial distribution functions as a function of the coordination number are displayed on Fig. 8 for the MCY water at 25 °C. The curve for the ST2 water is very similar and is not shown. There is a discontinuity at $R=R_M$ for all K reflecting the fact that if a molecule has less neighbors within a sphere of radius R_M than the average coordination number then it is very likely that there is one just outside the sphere and vice versa. There is no evidence of peak around 3.5 Å for $g(6,R)$ with either potentials, discounting the measurable existence of interstitial water for these water models.

VI. SUMMARY AND CONCLUSIONS

The description of liquid water in terms of pairwise additive MCY and ST2 potentials obtained in previous computer simulation studies has been supplemented by the present work in two ways. First, the temperature dependence of the description was studied in the range of 25–50 °C for the MCY water. Second, additional distribution functions have been presented for both the MCY and ST2 waters. As expected, the increase of the temperature causes a small but statistically significant loss of structuration. The new distribution functions provide further support of the continuum model by the

TABLE VII. The probabilities of finding a cavity of at least R_C as a function of the temperature, potential and R_C.

	$R_C > 2.4$ Å	$R_C > 2.6$ Å	$R_C > 2.8$ Å
MCY 25 °C	(1.41+0.08)E-2	(2.73+0.3)E-3	(3.20+0.7)E-4
MCY 37 °C	(1.45+0.07)E-2	(2.87+0.5)E-3	(3.64+2.0)E-4
MCY 50 °C	(1.46+0.06)E-2	(2.72+0.2)E-3	(3.41+1.0)E-4
ST2 10 °C	(2.91+0.08)E-2	(8.37+0.6)E-3	(17.77+1.7)E-4

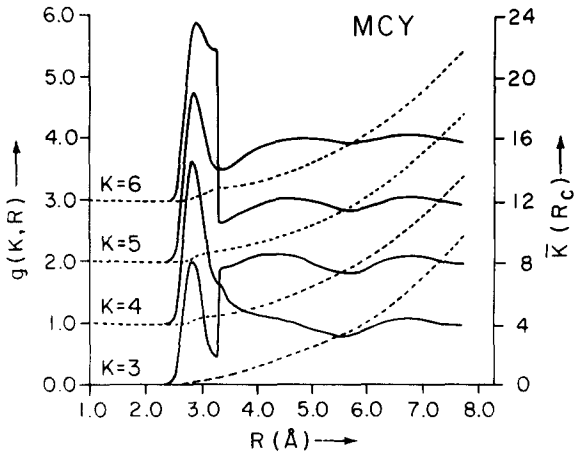

FIG. 8. Radial distribution functions (full line) and running coordination numbers (broken line) for water molecules with different coordination numbers for MCY water at $T = 25°C$. The curves belonging to different coordination numbers are shifted upwards by one unit each.

unimodal nature of the near-neighbor pair-energy distribution [in agreement with earlier results in the (T, P, N) ensemble results] and by the lack of any peak at 3.5 Å in the radial distribution function for water molecules with coordination number 6. It is to be emphasized, however, that the possibility exists that the inclusion of cooperative contributions might change this conclusion. Also, the importance of the dipolar forces was demonstrated through the distribution of near-neighbor dipole correlation function.

ACKNOWLEDGMENTS

This research was supported by a Grant No. 5-R01-GM-24914-5 and a CUNY Faculty Research Award.

[1]S. Swaminathan and D. L. Beveridge, J. Am. Chem. Soc. **99**, 8392 (1977).
[2]M. Mezei, S. Swaminathan, and D. L. Beveridge, J. Am. Chem. Soc. **100**, 3255 (1978).
[3]M. Mezei, S. Swaminathan, and D. L. Beveridge, J. Chem. Phys. **71**, 3366 (1979).
[4]M. Mezei and D. L. Beveridge, J. Chem. Phys. **74**, 622 (1981).
[5]A. Ben-Naim, *Water and Aqueous Solutions* (Plenum, New York, 1974).
[6]C. Matsuoka, E. Clementi, and M. Yoshimine, J. Chem. Phys. **64**, 1351 (1976).
[7]E. H. Stillinger and A. Rahman, J. Chem. Phys. **60**, 1545 (1974).
[8]D. L. Beveridge, M. Mezei, S. Swaminathan, and S. W. Harrison, in *Computer Modeling of Matter*, edited by P. G. Lykos (American Chemical Society, Washington, D.C., 1978) p. 191.
[9]D. L. Beveridge, M. Mezei, P. K. Mehrotra, F. T. Marchese, T. R. Vasu, and G. Ravi-Shanker, Ann. N. Y. Acad. Sci. (to be published).
[10]F. H. Stillinger, Science **209**, 451 (1980).
[11]H. A. Scheraga (to be published).
[12]G. C. Lie, E. Clementi, and M. Yoshimine, J. Chem. Phys. **64**, 2314 (1976).
[13]A. Ben-Naim, J. Chem. Phys. **52**, 5531 (1970).
[14]J. C. Owicki and H. A. Scheraga, J. Am. Chem. Soc. **99**, 7403 (1977).
[15]J. A. Pople, Proc. R. Soc. London Ser. A **205**, 163 (1951).
[16]M. G. Sceats, M. Stavola, and S. A. Rice, J. Chem. Phys. **70**, 3927 (1979).
[17]W. L. Jorgensen, Chem. Phys. Lett. **70**, 326 (1980).
[18]W. L. Jorgensen, J. Am. Chem. Soc. **101**, 2011 (1979).
[19]A. Geiger, F. H. Stillinger, and A. Rahman, J. Chem. Phys. **70**, 4185 (1979).
[20]B. Z. Gorbunov and Yu. I. Naberkuhin, J. Struct. Chem. (USSR) **16**, 703 (1975).
[21](a) C. S. Pangali, M. Rao, and B. J. Berne, Chem. Phys. Lett. **55**, 413 (1979); (b) M. Rao, C. S. Pangali, and B. J. Berne, Mol. Phys. **37**, 1779 (1979).
[22]A. H. Narten, J. Chem. Phys. **55**, 2268 (1971).